Continental Shelf Research, Vol. 8, Nos. 5–7, pp. 729–736, 1988.
Printed in Great Britain.

0278–4343/88 $3.00 + 0.00
Pergamon Press plc.

Tides near a shelf–slope front

HSIEN WANG OU* and LEO R. M. MAAS†

(*Received* 20 *February* 1986; *in revised form* 26 *February* 1987; *accepted* 12 *August* 1987)

Abstract—A two-layer model is used to examine the tides near a shelf–slope front that intersects both the bottom and the sea surface. Because of the presence of super-inertial eigenmodes in such a front, the semidiurnal tide is preferentially amplified (relative to the diurnal tide) by the generation of the baroclinic tide. Over the Mid-Atlantic Bight where the stratification is typically weak (i.e. the baroclinic radius of deformation is small compared with the width of the frontal zone), the baroclinic tide only slightly modifies the barotropic tide, it nevertheless causes a surface (bottom) intensification of the cross-shelf flow at the diurnal (semidiurnal) frequency. The model results compare favorably with observations and their implications on the tidal mixing in the frontal zone are discussed.

1. INTRODUCTION

IT IS well known that baroclinic tides can be generated by barotropic tides when the density surfaces are perturbed. This perturbation occurs when the barotropic tide encounters the topographic slope such as that near the continental marginal areas (BAINES, 1982) or when the density surfaces are slanted such as that in a frontal zone (CHUANG and WANG, 1981). In mid-latitudes, the baroclinic tide at semidiurnal frequency can radiate away from the generation area along characteristics and the outgoing energy flux depends on the local forcing as well as the ambient stratification.

In the Mid-Atlantic Bight, there is a density front situated near the shelf-break that separates the less dense shelf water from the slope water (Fig. 1). In the winter time, intense mixing due to surface cooling and atmospheric disturbances considerably weakens the stratification outside the frontal zone and hampers the outward radiation of the baroclinic tide. Standing modes are thus generated in the frontal zone that can resonate with the tidal forcing when the condition is favorable and greatly amplify the tidal amplitude and hence mixing within the frontal zone.

To assess this effect and, more generally, to examine the tidal fields near a shelf–slope front, we consider a two-layer model as formulated in Section 2. The eigenmodes of the front are discussed in Section 3 and the model results are compared with observations in Section 4.

2. THE MODEL

Let us consider a model configuration shown in Fig. 2. The front is approximated by a density interface that slopes in opposite sense from the topography and that intersects

* Lamont-Doherty Geological Observatory of Columbia University, Palisades, NY 10964, U.S.A.
† Institute of Meteorology and Oceanography, State University of Utrecht, Utrecht, The Netherlands. Present affiliation: Netherlands Institute for Sea Research, Texel, The Netherlands.

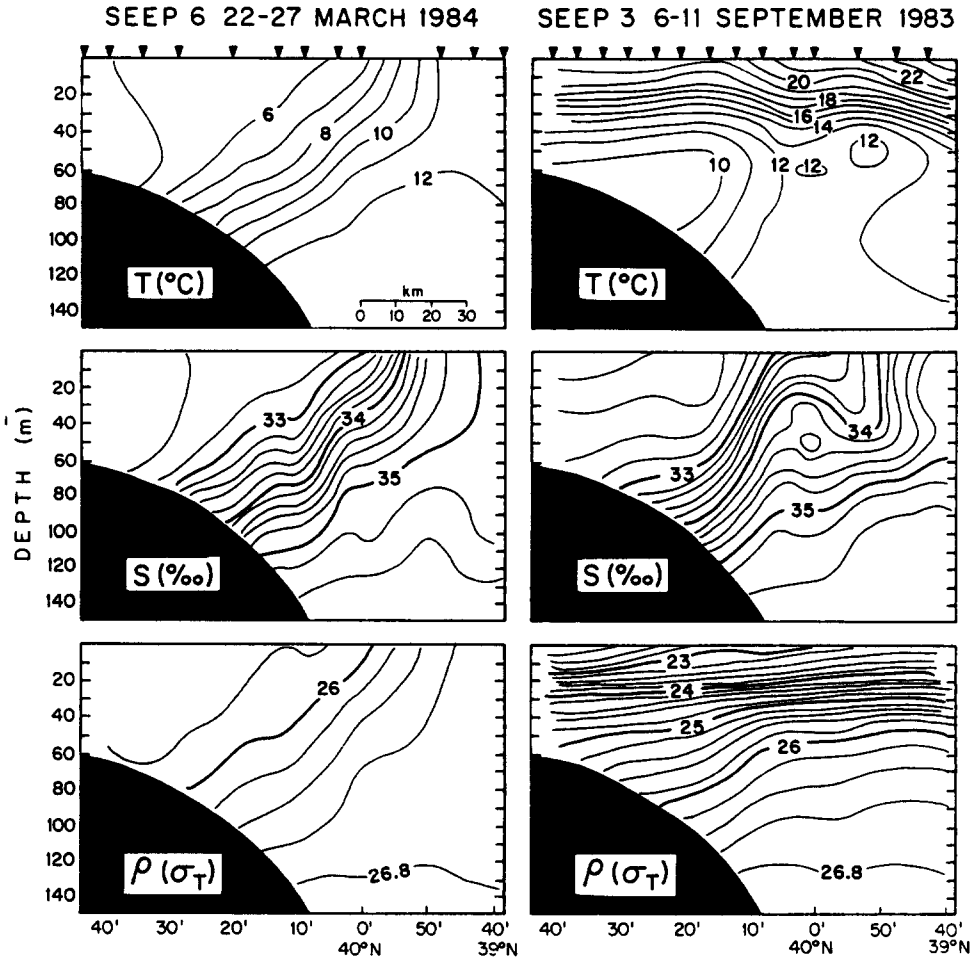

Fig. 1. Hydrographical sections showing the winter and summer frontal structure in the Mid-Atlantic Bight (data from SEEP—I, courtesy of C. Flagg and T. Hopkins).

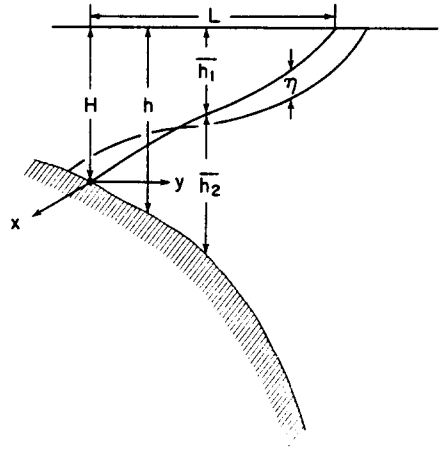

Fig. 2. The model configuration.

both the top and bottom surfaces. The current fields are assumed to be vertically uniform within each layer and all the field variables are assumed to vary in the cross-shelf direction only.

We assume the mean fields (denoted by overbars) to consist of a vanishing cross-shelf flow and a geostrophically balanced along-shelf flow so that, nondimensionally,

$$\bar{v}_1 = \bar{v}_2 = 0, \tag{2.1}$$

$$\bar{u}_1 - \bar{u}_2 = -\bar{h}_{1y}, \tag{2.2}$$

where subscripts 1 and 2 denote the variables in the upper and lower layer, respectively, and partial derivatives are indicated by subscripts throughout this paper. In the above equations, we have used the scaling rules (indicated by brackets) that $[y] = L$ (the width of the frontal zone), $[h] = H$ (the water depth at the shoreward edge of the front), and $[\bar{u}] = g'H(fL)^{-1}$ with g' being the reduced gravity across the frontal interface and f, the Coriolis parameter.

For tidal motions, we assume that the fluid is inviscid, adiabatic and hydrostatic, and that the surface is rigid so that the cross-shelf tidal transport Q is constant in y, then the tides at frequency $\sigma(\approx e^{-i\sigma t})$ satisfy the nondimensionalized equations,

$$-i\sigma u_1 + S^2 v_1 \bar{u}_{1y} - v_1 = 0, \tag{2.3a}$$

$$-i\sigma v_1 + u_1 = -p_{1y}, \tag{2.3b}$$

$$-i\sigma u_2 + S^2 v_2 \bar{u}_{2y} - v_2 = 0, \tag{2.3c}$$

$$-i\sigma v_2 + u_2 = -p_{2y}, \tag{2.3d}$$

$$p_1 - p_2 = S^2\eta, \tag{2.3e}$$

$$(\bar{h}_1 v_1)_y - i\sigma\eta = 0, \tag{2.3f}$$

$$\bar{h}_1 v_1 + \bar{h}_2 v_2 = 1, \tag{2.3g}$$

where η is the downward displacement of the frontal interface, and the additional scaling rules that $[\sigma] = f$, $[u, v] = Q/H$, $[p] = f[v]L$ and $[\eta] = [v]H(fL)^{-1}$ have been used. The only internal parameter is thus the Burger number S^2 defined as $(R_C/L)^2$, where $R_C \equiv (g'H)^{1/2}f^{-1}$ is the baroclinic radius of deformation.

If we define the barotropic (suffix T) and baroclinic (suffix C) tide as

$$v_T = (\bar{h}_1 v_1 + \bar{h}_2 v_2)/h, \tag{2.4}$$

and

$$v_C = v_1 - v_2, \text{ etc.}, \tag{2.5}$$

then the equations governing the two components can be derived from (2.3), which yield

$$v_T = 1/h, \tag{2.6}$$

and

$$-i\sigma u_C + S^2\left(\frac{\bar{u}_{1y}}{\bar{h}_1} + \frac{\bar{u}_{2y}}{\bar{h}_2}\right)\bar{h}_e v_C - v_C = -S^2(\bar{u}_{1y} - \bar{u}_{2y})v_T, \tag{2.7a}$$

$$-i\sigma v_C + u_C + S^2\eta_y = 0, \tag{2.7b}$$

$$(\bar{h}_e v_C)_y - i\sigma\eta = -(\bar{h}_1 v_T)_y, \tag{2.7c}$$

where $\bar{h}_e \equiv \bar{h}_1\bar{h}_2/h$ is the equivalent depth. It is seen that, because of the rigid lid assumption, the barotropic tide (v_T) varies inversely with the water depth, which generates the baroclinic tide through the advection of the mean vorticity shear (r.h.s. of equation 2.7a) and the perturbation of the density interface (r.h.s. of equation 2.7c). Using (2.2), the above equations can be reduced to a single equation governing the variable $V_C \equiv \bar{h}_e v_C$,

$$V_{Cyy} + \left(\frac{\sigma^2 - 1}{S^2\bar{h}_e} + \frac{\bar{u}_{1y}}{\bar{h}_1} + \frac{\bar{u}_{2y}}{\bar{h}_2}\right)V_C = F(y) \equiv \frac{\bar{h}_{1yy}}{h} - \left(\frac{\bar{h}_1}{h}\right)_{yy}, \tag{2.8}$$

with the boundary conditions that (since $\bar{h}_e$ vanishes at the end points),

$$V_C = 0 \qquad \text{at } y = 0 \text{ and } 1. \tag{2.9}$$

The forcing by the barotropic tide (F) thus consists of two terms derived, respectively, from the two terms on the r.h.s. of (2.7). It is seen that, because the mean current is geostrophic, the two terms are comparable and neither can be arbitrarily neglected. In fact, if the bottom is flat, the two terms exactly cancel out; i.e. a frontal interface can be rather convoluted and yet there is no forcing of the baroclinic tide by the barotropic tide. The result should also apply to a continuously stratified fluid, which points to the importance of topography in the generation of the baroclinic tide even when the isopycnals are not level. For a typical shelf–slope front that slopes upward and a bottom that increasingly steepens in the offshore direction, one can show that $F(y)$ is negative.

Since the homogeneous part of (2.8) and (2.9) constitutes the Sturm–Liouville eigenvalue problem,

$$V_{Cyy} + [\lambda r(y) - q(y)]V_C = 0, \qquad V_C(0) = V_C(1) = 0, \tag{2.10}$$

with

$$\lambda \equiv \frac{\sigma^2 - 1}{S^2}, \; r(y) \equiv \frac{1}{\bar{h}_e},$$

and

$$q(y) \equiv -\frac{\bar{u}_{1y}}{\bar{h}_1} - \frac{\bar{u}_{2y}}{\bar{h}_2},$$

there exists a denumerable sequence of eigenvalues λ_n, and the corresponding eigenfunctions V_n form a complete orthogonal set. The forced solution can thus be expanded in an infinite series (Courant and Hilbert, 1937)

$$\begin{aligned} V_C &= \sum_{n=1}^{\infty} \frac{c_n}{\lambda - \lambda_n} V_n \\ &= \sum_{n=1}^{\infty} \frac{S^2 c_n}{\sigma^2 - \sigma_n^2} V_n, \end{aligned} \tag{2.11}$$

where $c_n \equiv \int_0^1 F V_n dy$, and $\sigma_n = (1 + S^2\lambda_n)^{1/2}$ is the eigenfrequency of the system.

Resonance occurs when the forcing frequency σ approaches the eigenfrequency σ_n and the forced solution will be dominated by the nth eigenmode. In practice, because of the presence of dissipation, the denominator in (2.11) never really vanishes and since, for a slowly varying $F(y)$, c_n decreases rapidly with increasing n, generally only the first few terms need to be included in the expansion. To assess the resonance condition, we shall examine the eigenmodes in the next section.

3. THE EIGENMODES

For a general model geometry and mean flow field, the eigenmodes need to be calculated numerically. But to characterize the modal properties, we shall first consider the simpler case of a flat bottom and a mean flow with no lateral shear (within each layer), and then examine the effects of a varying topography and mean shear.

In the absence of lateral shear in the mean flow, $q(y)$ vanishes, and, because of geostrophy (equation 2.2), the frontal interface is straight with $\bar{h}_1 = 1 - y$. A flat bottom ($h = 1$) then implies that $\bar{h}_e = y(1 - y)$ and the eigenvalue problem (2.10) becomes

$$V_{Cyy} + \frac{\lambda}{y(1-y)} V_C = 0,\ V_C(0) = V_C(1) = 0. \tag{3.1}$$

Defining $W = V_{Cy}$ and $z = 2y - 1$, then W satisfies the Legendre's equation,

$$[(1 - z^2)W_z]_z + \lambda W = 0, \tag{3.2}$$

with the constraints that W be finite at the end points $z = -1$ and 1. The eigenvalues are thus given by

$$\lambda_n = n(n + 1), \tag{3.3}$$

or,

$$\sigma_n = [1 + S^2 n(n + 1)]^{1/2}, \tag{3.4}$$

and the eigenfunctions are the Legendre polynomials

$$W_n = P_n(z) \equiv \frac{1}{2^n n!} \frac{d^n}{dz^n} (z^2 - 1)^n. \tag{3.5}$$

In terms of the original variables, we then have

$$V_n = a_n \frac{d^{n-1}}{dy^{n-1}} [y(1 - y)]^n, \tag{3.6}$$

where a_n is a normalizing factor such that

$$\int_0^1 \frac{V_m V_n}{\bar{h}_e} dy = \delta_{mn}. \tag{3.7}$$

It is seen that the eigenfrequency σ_n increases with the mode number n, as well as the number of zero crossings (given by $n - 1$) of V_n within the interval (0, 1). Also, as expected, the eigenfrequencies have a lower cut-off at the inertial frequency and increase as the front stiffens (increasing S^2).

With a sloping bottom, $\bar{h}_e$ is everywhere greater but the change is expected small due to the fact that h_e is bounded by the smaller layer depth and hence is not overly sensitive to large increase of the water depth (a classical analog is the resistance for a pair of resistors in parallel). There is a theorem (COURANT and HILBERT, 1937, p. 411) stating that if $r(y)$ of (2.10) varies in one sense over the whole domain, every eigenvalue varies in the opposite sense. We thus expect the steepening bottom, by increasing $\bar{h}_e$ and decreasing $r(y)$, to slightly increase the eigenfrequency of (3.4). Physically, this is because the interface waves are travelling at a faster speed when $\bar{h}_e$ increases, resulting in higher frequency for the standing modes.

Since the mean current shear enters (2.10) through both the function $q(y)$ and, because of geostrophy, the function $r(y)$, its effect on the eigenfrequency in more subtle. But if both layers have the same mean vorticity so that $\bar{h}_1$ remains the same (see equation 2.2), then a cyclonic (anticyclonic) flow will increase (decrease) $q(y)$ while keeping $r(y)$ unchanged. Based on the theorem cited above which also states that if $q(y)$ varies in one sense over the whole domain, every eigenvalue varies in the same sense, the cyclonic (anticyclonic) flow therefore will increase (decrease) the eigenfrequency of (3.4). Physically, a cyclonic (anticyclonic) flow effectively enhances (reduces) the restoring force associated with the earth's rotation and hence increases (decreases) the frequency of the eigenmodes. From the above discussions, it is also clear that eigenfrequencies can be sub-inertial if the mean flow is sufficiently anticyclonic. If the frontal configuration changes as a result of the mean current shear, the net effect is less certain. For example, if the cyclonic vorticity is greater in the upper layer so that the front is convex upward (i.e. $|\bar{h}_{1y}|$ decreases offshore), then $\bar{h}_e$ is smaller which counters the effect of the cyclonic vorticity on the eigenfrequency. The net effect thus depends on the more detailed distribution of the flow field.

4. APPLICATION

In the Mid-Atlantic Bight, the frontal zone typically spans a distance of a few tens of kilometers (see e.g. Fig. 1) while the baroclinic radius of deformation is a few kilometers (using $g' \approx 0.2$ cm s^{-2}, $H \approx 100$ m and $f \approx 10^{-4}$ s^{-1}, one estimates that $R_C \approx 4.5$ km), the Burger number is thus generally small. From the above discussions, we deduce that the eigenfrequency for the low modes is near inertial and resonance at tidal frequencies might not be predominant. Nevertheless, because of the cut-off of the eigenfrequency at the inertial frequency, we expect the semidiurnal tide to be preferentially amplified (relative to the diurnal tide). Is there any observational evidence for this model prediction? During SEEP—I (Shelf Edge Exchange Processes), an array of thermistor chains were moored across the shelf-break south of Cape Cod to monitor the frontal motion. An empirical orthogonal function analysis in the frequency domain has been carried out to characterize the dominant thermal signals (OU *et al.*, 1988). The analysis showed that the dominant modes at the diurnal and semidiurnal frequency have quite different structures. Specifically, the diurnal mode has large spatial scales, reflecting the barotropic forcing, while the semidiurnal mode has smaller spatial scales and is more tightly bound to the front. Despite the sharply reduced coherence scales, the semidiurnal mode nevertheless accounts for as much percentage of the total variance as the diurnal mode. The analysis is consistent with the preferential amplification of the semidiurnal tide by the generation of the frontal modes.

Retaining only the low modes, the forced solution (2.11), in the asymptotic limit $S^2 \ll 1$, becomes

$$V_C \approx \sum_{n=1}^{\infty} \frac{S^2 c_n}{\sigma^2 - 1} V_n$$

$$= \frac{S^2 \bar{h}_e}{\sigma^2 - 1} F(y) \text{ (using the definition of } c_n \text{ and equation 3.7),} \tag{4.1}$$

or,

$$v_C \approx \frac{S^2}{\sigma^2 - 1} F(y). \tag{4.2}$$

This asymptotic solution can also be derived from (2.8) by dropping the V_{Cyy} term, which is equivalent to retaining only the low modes in the expansion (2.11). Since $F(y)$ is generally negative for the shelf–slope front (see Section 2), v_C is thus positive (negative) for the diurnal (semidiurnal) tide and the cross-shelf flow is surface (bottom) intensified (see equation 2.5).

We should point out that the asymptotic solution (4.1), although derived for the case when the front intersects both the top and bottom surfaces, remains valid even when the front has open ends. Assuming a localized forcing, then instead of vanishing baroclinic transport, radiation conditions must be imposed at the end points. The general solution to (2.8) is composed of a particular solution (the forced wave, equation 4.1) and a homogeneous solution (free waves) needed to satisfy the radiation conditions. For small S, the free waves have small lateral scales (nondimensionally of order S due to the balance of the first two terms in equation 2.8) and to satisfy the radiation condition that matches both V_C and its spatial gradient (equivalently the frontal displacement) across the open boundary, the free waves must have small amplitude compared with the forced wave (the ratio being of the order S). This result applies for both the progressive (semidiurnal) and evanescent (diurnal) waves, the asymptotic solution (4.1) thus remains the dominant response for an open front.

To check the model prediction regarding the vertical structure of the cross-shelf flow, we use the current data of the Nantucket Shoals Flux Experiment (Beardsley *et al.*, 1983). We have plotted in Fig. 3 the location of the current meter measurements at their mooring 5 and the mean position of the winter front. Numbers listed alongside are the amplitude of the cross-shelf flow (in cm s^{-1}) of the two dominant tidal constituents together with their averages within each layer. Notwithstanding large statistical errors, the diurnal tide does appear to be surface intensified while the semidiurnal tide bottom intensified, in agreement with the model prediction. Taking $\bar{h}_1 \approx \bar{h}_2$, estimates for the baroclinic tide, the barotropic tide and their ratio are also listed. According to the asymptotic solution (4.2), this ratio should be three times greater for the diurnal tide (with $\sigma \approx 0.75$) than for the semidiurnal tide ($\sigma \approx 1.5$). The opposite trend observed is thus suggestive of the preferential amplification of the semidiurnal tide as discussed above.

The preferential amplification and bottom intensification of the semidiurnal tide tend to enhance its role in the mixing process especially near the bottom. In addition, since the

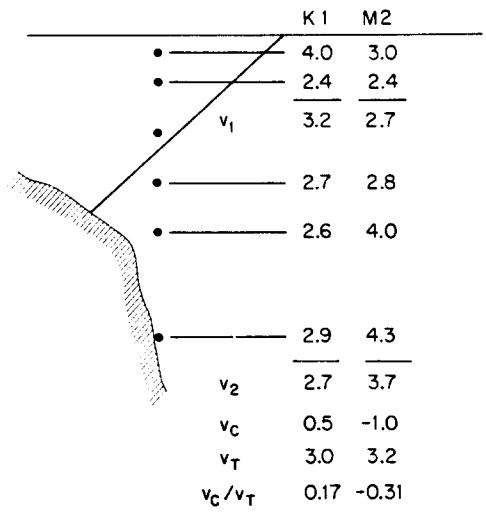

Fig. 3. Location of the current meters (in solid dots) at mooring number 5 of the Nantucket Shoals Experiment, as well as the mean position of the front (in solid line). Numbers listed are the amplitudes of the cross-shelf flow (in cm s^{-1}) at two dominant tidal constituents (taken from Table 11 of BEARDSLEY *et al.*, 1983), their averages within each layer, the estimated baroclinic and barotropic component (assuming equal upper and lower layer depth), and their ratios.

amplitude of the baroclinic tide depends on the frontal configuration, it can be regulated by low-frequency forcings. For example, a downwelling favorable wind which steepens the front and increases the Burger number, can amplify the tide and hence the mixing within the frontal zone.

Acknowledgements—The authors want to thank J. T. F. Zimmerman for pointing out the importance of mean vorticity shear in the generation of baroclinic tides, and R. C. Beardsley for useful comments. L. R. M. Maas appreciates the support of the Netherlands Organization for the Advancement of Pure Research (Z.W.O.) which enabled him to visit the Lamont-Doherty Geological Observatory during the conduct of this research. H. W. Ou is supported by the Department of Energy under Grant DE-AC02-76EV02185FX. Lamont-Doherty Geological Observatory Contribution No. 4249.

REFERENCES

BAINES P. G. (1982) On internal tide generation models. *Deep-Sea Research*, **29**, 307–338.

BEARDSLEY R. C., C. A. MILLS, J. A. VERMERSCH, Jr, W. S. BROWN, N. PETTIGREW, J. IRISH, S. RAMP, R. SCHLITZ and B. BUTMAN (1983) Nantucket Shoals Flux Experiment (NSFE79), Part 2: Moored Array Data Report. WHOI Technical Report, 140 pp.

CHUANG WEN-SSN and DONG-PING WANG (1981) Effects of density front on the generation and propagation of internal tides. *Journal of Physical Oceanography*, **10**, 1357–1374.

COURANT R. and D. HILBERT (1937) *Methods of mathematical physics*, Vol. 1, Interscience Publishers, New York, 560 pp.

OU H. W., F. AIKMAN III and R. W. HOUGHTON (1988) Complex empirical orthogonal function analysis of thermistor chain data near a shelf-slope front. *Continental Shelf Research*, **8**, 711–728.